THE JOURNAL OF PHYSICAL CHEMISTRY C

Article

pubs.acs.org/JPCC

Gold Cluster Electronic Radiative Cooling and Abundances

Klavs Hansen,*[,†,‡] Piero Ferrari,[§] Ewald Janssens,[§] and Peter Lievens[§]

[†]Tianjin International Center of Nanoparticles and Nanosystems, Tianjin University, Tianjin 300072, P. R. China

[‡]Department of Physics, University of Gothenburg, 41296 Gothenburg, Sweden

[§]Laboratory of Solid State Physics and Magnetism, KU Leuven, 3001 Leuven, Belgium

ABSTRACT: The effect on abundances of radiative cooling of gold clusters is analyzed quantitatively for cluster sizes n = 8−20 based on known dissociation energies, radiative time constants and the monomer unimolecular decay frequency factor, and an assumed dimer loss frequency factor. Radiative cooling is observed to quench the temporal development of the abundance spectra and, in general, to produce larger size-to-size contrasts than observed in the absence of radiation. Also, the emission of photons with large and small energies was compared quantitatively. For small photon energies, the radiative time constant is not given by the photon emission rate constant. An alternative expression for this regime was found to be very accurate. Strong radiative cooling will have consequences both for the interpretation of mass abundance spectra and potentially also for the production of specific mass selected nanoparticles. The present work supplies the conceptual framework for such applications.

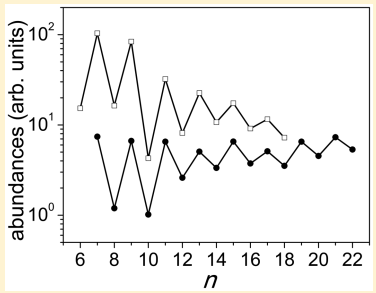

INTRODUCTION

Gold clusters have attracted much interest due to their high chemical reactivity and their potential use as catalysts.[1−3] These applications usually require the clusters to be deposited. However, the properties of clusters are arguably best studied in their pure form in gas phase, free of the perturbing influence of a substrate that adds another layer of complication to the already difficult theoretical description of the quantum-mechanical structure of this element. A range of experimental data is available for gas-phase gold clusters, mainly for the charged species. Spectroscopic studies have determined the gas-phase optical absorption cross sections in the visible and ultraviolet domain[4−6] for cold and small clusters and for neutral, deposited clusters.[7] In closely related studies, the surface plasmon has been studied intensely for larger and deposited clusters.[8] Mobility studies have determined geometric sizes,[9] which is also of relevance for the calibration of quantum theoretical methods.

In refs 10 and 11, cationic separation energies, that is, differences in ground-state energies of neighboring cluster sizes, were given. The values were determined with an experimental protocol that eliminates virtually all model dependence. These numbers have direct importance as benchmark values for the quantum chemical computations that build on energy optimization. They are also important in the description of gas-phase studies and for studies of other thermal properties of these clusters.

Recently, it was discovered that highly excited gold clusters emit thermal radiation with rates that are orders of magnitude higher than rates corresponding to vibrational transitions.[12] Several other recent studies have shown that these thermal radiative cooling times can be very short compared with infrared radiative time constants for clusters of the elements silicon,[13] niobium,[14] and carbon[15,16] as well as for the PAH molecular ion anthracene.[17] We expect this phenomenon will turn out to be a general feature of clusters with delocalized valence electrons. The values of the radiative time constants for the cationic gold clusters n = 6−13, 15 have a geometric average around 10^5 s^{-1}.[12]

Applications of thermal radiative relaxation have been envisioned for clusters of refractory metals,[18,19] and observation of this radiation adds interest to these applications. From a fundamental point of view and from the point of view of production of nanoparticles, one of the most interesting aspects of the radiation is the strong size dependence. This is seen very clearly in the gold radiation constants, where the odd−even effect is very pronounced and where the values drop several orders of magnitude above n = 15.[12] The radiation originates in thermally excited electronic states, a type of fluorescence predicted in ref 20 long ago. The radiative rate constant for clusters of sizes n = 6−13, 15 have been measured experimentally, whereas the sizes n = 14, 16−20 have radiative constants too low to give reliable values. We will use their fitted values with the understanding that these values may not correspond to the numbers that will be measured in a device with a more extended time range.

The thermal (activated) nature of the radiation process, in combination with limits on the emission strength, places rigorous upper limits on the energies of the excited states. The emission is limited by the Thomas−Reiche−Kuhn sum rule for the oscillator strength for absorption.[21] By detailed balance,

Special Issue: ISSPIC XVIII: International Symposium on Small Particles and Inorganic Clusters 2016

Received: October 3, 2016
Revised: November 23, 2016
Published: December 23, 2016

DOI: 10.1021/acs.jpcc.6b09998
J. Phys. Chem. C 2017, 121, 10663−10669

limits on absorption place equivalent limits on the emission rate. We expect the excited-state energies are located in the infrared, that is, in an energy regime where the standard method of action spectroscopy has historically experienced difficulties because of the reduced quantum yield after absorption of low-energy photons, although the development of the intense free electron lasers has greatly expanded the possibilities of this tool; see, for example, refs 22 and 23. The spectroscopic studies in the literature[4−7,24] have mapped the visible and near-infrared regime, and these studies are of minor relevance for the radiative cooling of excited clusters. We are therefore left with the precise state energies as free parameters. Also, the oscillator strengths are free parameters, but they are, for a given cluster size, related to the transition energy by the observed radiative time constant.

We have studied the effect of radiative cooling and its size dependence in simulations of decays of highly excited gold clusters with the aim of gaining an understanding of the relative importance of cluster stability and radiative cooling for the shape of the abundance spectrum. The well-characterized gold clusters make them good objects for this type of study. In addition to the radiative constants, the relevant data available in the literature for the cationic clusters include dissociation energies for monomer loss for clusters n = 7−22, dissociation energies for dimer loss for n = 9, 11, 13, 15, the monomer rate constant frequency factor, and the branching ratios of dimer/monomer dissociation. We will not fix the magnitude of the photon energy in the simulations. As will be discussed below, there are two cases, for large and small photon energies. Both will be analyzed numerically.

For clusters prepared hot and allowed to cool freely, evaporation of massive particles (atoms/dimers/electrons) is initially the dominant energy loss process. After some time, when enough energy has been lost by evaporation of atoms, radiative cooling becomes the dominant decay channel. This is a general feature of these competing processes. It is readily understood as the consequence of the different frequency factors and decay activation energies in the two types of processes. Atomic evaporation has both higher frequency factors and activation energies than photon emission. This causes the atomic emission to dominate at high excitation energies and photon emission at low energies. As the clusters cool freely, the excitation energy is progressively reduced, with a logarithmic time dependence, and at some point in time the dominant decay therefore changes from atomic evaporation to photon emission. The crossover time from a predominantly unimolecular decay to the radiative cooling regime defines the radiative cooling time.

The need for a numerical simulation, as opposed to an analytical derivation, when estimating the influence of radiative cooling on the cluster abundances, is due to the presence of competing unimolecular decay channels. For several gold cluster sizes, both monomer and dimer evaporation occurs, and this renders an analytical solution of the problem so complicated that presently only a numerical solution is feasible.

EXPERIMENTAL PROCEDURES

The experimental apparatus and procedure are identical to the ones described in detail in refs 13 and 14. In brief, the clusters were produced in a laser vaporization source,[25] operated with a pulsed Nd:YAG laser (532 nm, 10 Hz) with pulse energies of 15−25 mJ. The ablated material was cooled with a pulse of helium gas, which carried the clusters through a skimmer and into the primary acceleration region of the time-of-flight (TOF) mass spectrometer.

The charged clusters produced in the source were rejected from the acceleration region by a small positive potential on the first extractor grid downstream from the source. Negative ions from the source were not accelerated toward the detector and therefore not observed.

The neutral cluster beam present in the TOF primary acceleration region, where the electric fields are initially switched off, was ionized and photofragmented by a pulse of UV light (third harmonic of a Nd:YAG laser, 355 nm, 10 Hz). This laser pulse is short, on the order of ten nanoseconds, and can be considered a delta function in time in the following. The time it takes to mass-select the clusters in the acceleration is denoted t_1. After acceleration the ions move toward a reflectron, which they reach after a flight of approximately a meter in a field-free region at ground potential. The time from absorption of the laser pulse to the entry into the reflectron is denoted t_2. The reflectron contains two fields, a short and strong entry field and a longer and weaker field, where the clusters spent most of their time inside the reflectron. After exit from the reflectron the ions fly another field-free distance before hitting the detector. By detuning the field in the reflectron, it is possible to measure the amount of metastable decay. This is used to quantify the radiative cooling with procedures that have been described in detail elsewhere (see, for example, refs 13 and 14). The measurements allow us to probe the abundances for the two times t_1 and t_2 with a single experiment.

SIMULATION PROCEDURES

The simulations were of the Monte Carlo type. A series of clusters was followed from initially large sizes with large excitation energies as they decayed sequentially in processes where atoms, dimers, or both are lost and radiation is emitted, leading to both a gradual reduction of the excitation energy and the size. The size of a cluster in one of these decay chains was sampled at predetermined times. The time-dependent abundance spectra were constructed by calculating a large number of decay chains. The decays were assumed to be completely statistical and the state of a cluster, and hence its decay rates, determined solely by its excitation energy. We disregarded differences in rate constants for different angular momenta. No conserved quantity beyond energy then needed to be considered. The assumption of statistical decay simplified the simulations considerably because it was then not necessary to simulate the detailed time development of the state of a cluster. The elementary processes in a decay chain were

$$\mathrm{Au}_n^+(E) \rightarrow \mathrm{Au}_{n-1}^+(E - D_{n,1}) + \mathrm{Au} \quad (1)$$

$$\mathrm{Au}_n^+(E) \rightarrow \mathrm{Au}_{n-2}^+(E - D_{n,2}) + \mathrm{Au}_2 \quad (2)$$

$$\mathrm{Au}_n^+(E) \rightarrow \mathrm{Au}_n^+(E - h\nu) + h\nu \quad (3)$$

with the relevant total excitation energies given as arguments. We will use the terms dissociation energies, separation energies, and evaporative activation energies interchangeably here and represent them with the parameters $D_{n,i}$, i = 1,2. The measured D values were in all cases the excitation energy that was consumed in an evaporation process, and these energies are the ones that determine the rate of the activated process. In particular, none of the experimentally determined numbers from refs 10 and 11 need to be modified. The only

DOI: 10.1021/acs.jpcc.6b09998
J. Phys. Chem. C 2017, 121, 10663−10669

consequences of a reverse activation barrier would be the addition of a constant term to the kinetic energy release in the evaporative processes, and these are not sampled here.

The rate constant for monomer evaporation will be calculated as

$$k_{n,1} = \omega_1 \left(\frac{E - D_{n,1} + (3n-9)\hbar\omega_D/2}{E + (3n-6)\hbar\omega_D/2} \right)^{3n-7} \quad (4)$$

The expression is based on the high-energy next-to-leading order expression for the level density of a particle of harmonic oscillators with the average quantum energy $\hbar\omega_D$ = 165 K. Although such a level density is a simplification, the expression for the rate constant will be very accurate in the relevant energy range because it was the same expression that was used to extract the frequency factor in ref 11. Any errors will to first order be absorbed into that parameter. Similarly, the power $3n - 7$, common to both numerator and denominator, is an approximation that is valid for the same reason. Moreover, a common frequency factor can be used for all cluster sizes without significant loss of accuracy. It was determined to $\omega_1 = 2.4 \times 10^{15}$ s^{-1}.[11]

Dimer evaporation is present for cationic gold clusters of the sizes n = 7, 9, 11, 13, and 15.[26] The frequency factor for this channel is in general different from the monomer channel and must be determined independently. We use the experimental dimer dissociation energies and the abundances to determine the frequency factor. It is calculated as a single value for all cluster sizes, by analogy to the monomer case, by adjusting simulated abundances of, in particular, n = 8,10,12,14 to agree with the experimentally observed values. A larger dimer frequency factor gives lower abundances of these clusters and vice versa without changing other abundances significantly. The common value of the dimer evaporation frequency factor is set to $\omega_2 = 2.4 \times 10^{17}$ s^{-1}, that is, a factor 100 larger than the monomer frequency. By analogy to the monomer case and for simplicity, the level density of the product has been used with the same power as the precursor, viz. $3n - 7$.

Although the dimer frequency factor may seem high compared with standard values derived from, for example, RRKM theory, the nature of the expected transition state renders it plausible, and it is worth attaching a few words on this. Formulated in terms of the attachment cross section for the inverse process, application of detailed balance[27] supports the high value relative to the monomer evaporation value. The single most important difference between the monomer and dimer frequency factor is due to the dimer rotation. The value of the rotational constant of the $^{197}Au_2$ dimer is 0.028 cm^{-1},[28] corresponding to a rotational temperature of 0.040 K. With a product cluster temperature typically above 1000 K for decays on time scales of microseconds, the rotational partition function contributes a significant factor to the frequency factor, between 10^4 and 10^5, even if the energy carried away in the rotational degrees of freedom is only on the order of the temperature of the product cluster. In contrast, the vibrational frequency is on the order of 165 K, and the loss of vibrational states in an evaporative process is therefore on the order of a factor $(1000\ \text{K}/165\ \text{K})^2 \simeq 40$. The power 2 arises as the difference between the number of product vibrational degrees of freedom in monomer and dimer evaporation, $3n - 9$ for monomer evaporation versus $3n - 12 + 1$ for dimer evaporation. A ratio of the dimer and monomer evaporation frequency factor of 10^2, as used here, is therefore in fair agreement with expectations.

The dimer dissociation energy for n = 7, $D_{7,2}$, is unknown from experiments, as are the values for smaller clusters. Thus only the total rate constant of Au_7^+ is of interest here. We calculate that as the monomer rate constant multiplied by one plus the measured branching ratio between dimer and monomer evaporation, R. The latter is energy-dependent. We use the value for the highest energy measured, R = 24, and then multiply the monomer rate constant with the factor $1 + R = 25$.

For cluster sizes beyond those measured, dissociation energies were set to $D_{22,1}$ for $n > 22$ and $D_{7,1}$ for $n < 7$, and the radiative cooling time constant was set to infinity for these sizes. The smaller clusters may radiate strongly, but they are downstream in decay chains from the sizes shown in the Figures, and their decay consequently has no influence on the larger clusters.

The initial cluster distributions were generated with a flat size distribution between n = 3 and 40 and Gaussian energy distributions with mean $9n/20 + 15$ eV and a standard deviation of 2 eV. This ensured that the overwhelming part of clusters has the energy to evaporate at least once. For completeness we mention that the kinetic energy release was included in the simulations and set to twice the product temperature, corresponding to an energy-independent capture cross section. This energy loss is small and the specific choice is of little consequence here.

The photon emission rate constants were set to a constant for each cluster size. Given the strong dependence of the evaporative rate constant on energy, all evaporation processes apart from the last one occurred on such short times that very little is radiated during this time. The small amount that did occur could then be represented by the constant, final rate with little loss of accuracy.

In one part of the simulations, the photons were emitted with a preset energy of 1 eV, causing the emission of one photon to quench any further atomic evaporation. In this situation, the decay proceeds as[16]

$$I_n \propto \frac{e^{-k_{p,n}t}}{t} \quad (5)$$

where $k_{p,n}$ is the photon emission rate constant. The power law appears due to the broad initial energy distribution. In the other part, small photon energies, of 0.01 eV, were simulated to examine the behavior in a continuous cooling regime. For this situation, that is, the continuum limit, the decay has the profile

$$I_n \propto \frac{1}{e^{t/\tau_n} - 1} \quad (6)$$

Here τ_n is a time constant which is different from $k_{p,n}^{-1}$. The two expressions behave similar, as a plot of the two will demonstrate, but the interpretation of the radiative time constants is different. For the continuum emission limit, the measured/simulated time constant is calculated as[13]

$$\tau_n^{-1} = \frac{d \ln k_a}{dE} P \quad (7)$$

where k_a is the atomic emission rate constant (or a properly weighted value if there is more than one channel present), E is the excitation energy, and P is the emitted power

$$P = k_p h\nu \quad (8)$$

DOI: 10.1021/acs.jpcc.6b09998
J. Phys. Chem. C 2017, 121, 10663−10669

where k_p is the true photon emission constant. The two regimes are separated by the criterion on the evaporative rate constant, k_a, and the photon energy

$$h\nu \frac{\mathrm{d}\ln(k_a)}{\mathrm{d}E} = 1 \tag{9}$$

Photon energies higher than this will cause quenching decays, and lower energies correspond to continuum cooling. A calculation shows that with the photon energy of 0.01 eV the continuum cooling condition was fulfilled for all sizes in this study. The emission rate constant required in the simulation in order for τ to be equal to the measured time constant is then

$$k_{p,n} = \tau_n^{-1} \frac{D_n(3n-7)}{0.01\ \mathrm{eV}\ \ln(2.4 \times 10^{15}\ \mathrm{s}^{-1} t)^2} \tag{10}$$

In this expression, the measurement time is set to the experimental mass selection time, and the monomer frequency factor was used for simplicity.

The random numbers used in the simulation were either evenly distributed, Gaussian or exponential. The equidistant numbers were sampled from the compiler supplied subroutine, which has been checked for mean value, variance, and correlation between consecutive values. The Gaussian and the exponential distributions were generated as prescribed in ref 29. A total of 10^7 decay chains were started for each set of parameters. The statistical errors can be ignored.

RESULTS AND DISCUSSION

As a first result, we compare the simulated spectra with the experimentally observed abundances to identify any deviation caused by possible erroneous assumptions in the modeling. The comparison is shown in Figure 1, with $h\nu$ = 1 eV used for the simulations. It should be kept in mind that the comparison of experimental and simulated data does not extend to the general envelope of the abundance distribution because that is a function of source conditions and other parameters extrinsic to the clusters. Basically only the size-to-size variations can be compared. The clusters are produced and photoexcited, as described in the Experimental Procedure section. The detuning of the reflectron voltages was used to determine the abundances at two sets of times. The two experimental times were $t_1 = 0.77 \cdot \sqrt{n} + 0.93$ μs, corresponding to the acceleration time in the field, and $t_2 = 22.7 \cdot \sqrt{n} + 1.1$ μs, corresponding to the time needed to reach the reflectron after excitation. The offsets in these expressions are due to the speed of the clusters from the source.

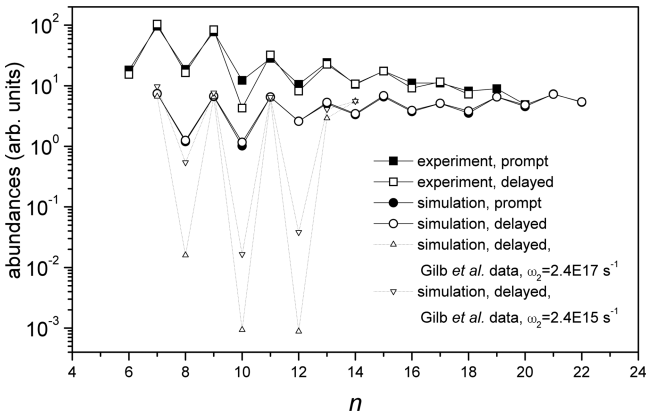

Figure 1. Experimental abundances (squares) and numerically simulated (circles) mass spectra. The experimental spectra were measured in a time-of-flight mass spectrometer. Filled squares: as extracted in the primary acceleration ("prompt"). Open squares: measured before entry into the reflectron ("delayed"). Filled and open circles: simulation results for the same times using dissociation energies as determined in ref 11 and radiative constants from ref 12. The photon energy was set to 1 eV in these simulations. Also shown are results of two simulations with the calculated dissociation energies from ref 9: one with a dimer frequency factor of 2.4×10^{17} s^{-1} (up triangles) and one with a dimer frequency factor of 2.4×10^{15} s^{-1} (down triangles). Experimental error bars based on reproducibility are on the order of the symbol size. Simulation error bars are negligible. All simulated data are rescaled with the same factor to provide values that can be compared with the experimental results.

The data for long times compare very well with similar data from sputter sources[30] and from experiments where the preproduced cationic clusters are laser-heated.[31] Also, the agreement between the experimental and simulated data is, in general, good, considering the self-imposed restriction to use a single universal frequency factor. (The overall intensity is obviously not of relevance here, and the smooth variations depend on non-cluster-specific quantities, as mentioned above.) For all but n = 10, the abundances at t_1 and t_2 are practically identical. The difference between the two values for n = 10 can be traced to the ratio of dissociation energies $D_{11,1}/D_{10,1}$ = 1.6, which is the biggest for all of the clusters studied here, together with the absence of any decay from n = 11 to 10. Please consult Chapter 6 of ref 32 for details. The experimentally observed behavior corresponds to a ratio of $D_{11,1}/D_{10,1}$ = 1.84, which differs from the ratio 1.6 observed here by a little more than one standard deviation.

The agreement between the experimental and simulated data is nontrivial. This point should be borne out when we compare the experimental abundances with simulated ones using the dissociative activation energies of ref 9 and parameters otherwise identical to the ones used above. Such a simulation is shown in Figure 1 together with another simulation, also based on the activation energies of ref 9 but with a dimer evaporation frequency factor that was reduced to the monomer value. Both curves strongly disagree with the experimental results. Agreement between the simulated and measured abundances for this set of dissociation energies would require an unphysical reduction of the dimer frequency factor by a further three orders of magnitude.

After having established that our input data from ref 11 and the chosen dimer frequency factor do indeed reproduce the important features of an evaporative mass spectrum, we proceed with systematic variations of the parameters in the problem. We will address two issues. One is the effect of radiation on the spectrum. The second is how the difference between the large and the small photon energy manifests itself in the abundances.

The measured radiative time constants[12] span several orders of magnitude, between the shortest time of n = 9, which is close to a microsecond, to values beyond the dynamic range of the mass spectrometer, which is on the order of one hundred microseconds. As a first study, the mass spectrum sampling time is varied from far below to far beyond the shortest and longest of these times. Both the situations with and without radiative cooling were simulated.

Figure 2 shows the outcome of the simulations. The sampling times were varied from 1 ns to 1000 s equidistantly on a logarithmic scale. The effect of radiation is most clearly

DOI: 10.1021/acs.jpcc.6b09998
J. Phys. Chem. C 2017, 121, 10663−10669

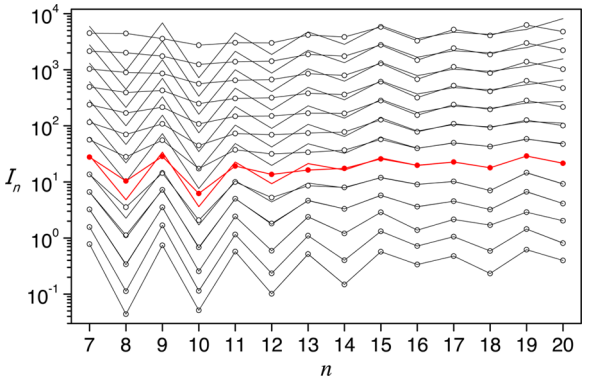

Figure 2. Simulated abundances after the times 10^q s, $q = -9, -8, ..., 3$. The spectra in the Figure are shifted a constant factor in the ordinate for display purposes with the shortest times at the bottom, and the absolute magnitude is arbitrary. Open circles represent nonradiating clusters, and radiating cluster are given by lines. The experimentally relevant comparison at 100 μs is curve number six from the bottom, given in red and with filled circles for the nonradiative simulation results.

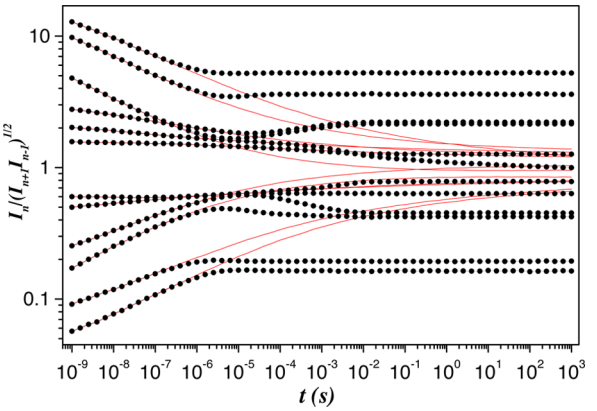

Figure 3. Contrasts in the simulated abundances shown in Figure 2 as a function of time. Circles represent radiating clusters; nonradiating clusters are given by lines. Values below unity correspond to low intensities and vice versa. The curves represent, at $t = 1$ ns from top to bottom, $n = 9$, 11, 13, 15, 19, 17, 16, 18, 14, 12, 8, and 10.

seen for small clusters, where one observes a strong size-to-size variation in the abundances of neighboring sizes at the short times. This contrast gradually disappears for the simulation of nonradiative clusters, whereas the radiative clusters retain contrast for all times.

The behavior of both sets of curves is easily understood qualitatively with reference to the results derived for abundances produced for nonradiative clusters with monomer evaporation only. With some additional conditions, primarily a constant cluster heat capacity for a given size, which are fulfilled for the present simulations, the abundances are[32]

$$I_n \propto \frac{1}{2}(D_n + D_{n+1}) + \frac{C_v}{\ln(\omega_1 t)}(D_n - D_{n+1}) \quad (11)$$

The largest part of the contrast between sizes is caused by the difference term on the right-hand side, for all but the smallest clusters. This term *decreases* with time, somewhat counterintuitively. In the presence of dimer evaporation, the relations are more involved and at present there is no simple closed expression for this, but the fundamental dependence on time is similar, i.e. the abundance contrasts decrease with time. This is also what is observed in the long time simulations in Figure 2. In the presence of radiation, however, this decrease is stopped at the time where all involved decays are quenched by the radiation.

This is illustrated in Figure 3, where the quantity $I_n/\sqrt{I_{n+1}I_{n-1}}$ is plotted versus time for data from the same simulation. This representation displays the effects of the radiative quenching more clearly and has the advantage relative to a plot of the raw intensities that both the zeroth and the first derivative of the (logarithm of the) abundance distributions with respect to cluster size cancel. The nontrivial behavior of the curves convincingly demonstrates the need for numerical solutions for this type of problems, and we also clearly see the general decrease in abundance contrast with time as well as the quenching effect on this by the radiative cooling. An additional observation should be made. The two highest values at the sampling time 1 ns belong to $n = 9$ (largest) and 11 (second largest), and the two lowest belong to $n = 8$ (lowest) and 10 (second lowest). $n = 8$, 10 are only populated from decays of $n = 9$, 11, respectively. Their radiative decay constants differ by a significant amount, by a factor 13 between $n = 8$ and 9 and by a factor 2.7 between $n = 10$ and 11. Despite this difference, the slow, logarithmic decrease in the abundance variations with time in eq 11 produce a practical identical freeze-out time for the abundances. In other words, although the quenching time determines the abundances, it is not a very critical dependence, and the precise freeze-out time is therefore not an essential parameter in the determination of the abundances. It is clear from Figure 2, however, that radiation does indeed play an important role in determining the ultimate shape of the spectra.

These conclusions are expected to hold for other small clusters or, more precisely stated, for other clusters with small heat capacities. As the cluster size and consequently also the heat capacity increases, one reaches a regime where the evaporation rate is so high that differences in time constants of this magnitude will cause a significant effect. Specifically, ratios of time constants of exp(1) are expected to become important when the heat capacity reaches the value $\ln(\omega t)^2/k_B$.[32] This heat capacity corresponds to a couple of hundred atomic monomers and half that value for molecular monomers. For even larger clusters, ratios even closer to unity will be relevant.

Turning now to the question of the effect of the magnitude of the energies of the photons emitted, we have compared the abundances from simulations with two different photon energies. The first is the high-energy value of 1 eV already presented above. The other simulations were made with a photon energy of 0.01 eV, corresponding to a continuum description, using the conversion given in eq 10 between observed quenching rate τ_n and the simulated low-energy photon emission rate constant k_p. The sampling time is set to 1 μs, which is close to the extraction time for the ions in the time-of-flight mass spectrometer. The result of the simulation is shown in Figure 4. No postsimulation adjustments have been made to either data set to obtain the close agreement in the Figure. The main difference between the two curves is a slightly smaller odd−even variation for the 0.01 eV photon energies for the smaller clusters and a slightly larger one for the larger clusters. In conclusion, we see that the suggested connection between the small photon energy cooling rate and the high-energy photon rate constants reproduce radiative effects on the abundance pattern.

DOI: 10.1021/acs.jpcc.6b09998
J. Phys. Chem. C 2017, 121, 10663−10669

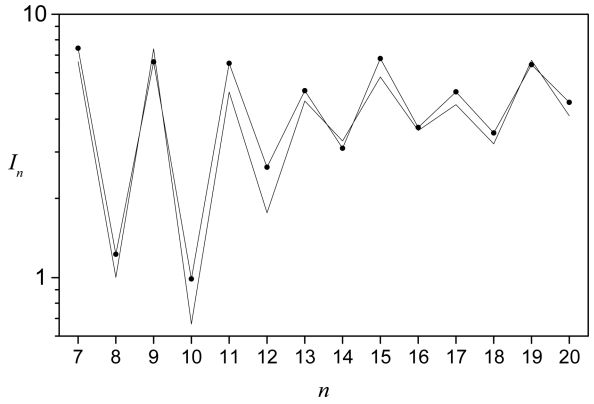

Figure 4. Comparison of the abundances at 1 μs for big (1 eV) (line) and small (0.01 eV) (line and filled circles) photon energies. The former data are the same as plotted in the fourth curve from the bottom in Figure 2.

SUMMARY

We have performed numerical simulations of the abundances of gold cation clusters in the size range n = 8−20 based on known dissociation energies, radiative time constants, and the monomer unimolecular decay frequency factor. The only parameter assumed was the dimer unimolecular decay frequency factor, which was adjusted to reproduce experimental cluster abundances. Only sizes n = 7, 9, and 11 were affected by the adjustment. The numerical value was found to be slightly lower than the detailed balance value but still two orders of magnitude higher than the monomer frequency factor. An alternative set of dissociation energies from the literature was tested but found to be inconsistent with the measured abundances.

The abundance spectrum develops with time after excitation with abundance contrasts that decrease with time. The radiative cooling was observed to quench this decrease and seen to influence the abundances strongly. In the first approximation it can be mimicked by fixing the abundances of a nonradiative spectrum at the freeze-out time. An unexpected result was that the detailed time of quenching, that is, the precise value of the radiative time constant, is relatively unimportant in this process. The reason for this can be traced to the relatively small evaporation rate for the small clusters studied here. For larger clusters this will be different because evaporation rates vary approximately proportional to the cluster heat capacity. These conclusions hold for situations both with and without dimer decays present.

Finally, the descriptions of the quenching for large and small photon energies were compared, and the expression for the continuum time constant was verified. It involves the logarithmic derivative of the unimolecular atomic emission rate constant with respect to energy and the photon energy.

The simulations presented here have been performed on cationic gold clusters. These species are well characterized with respect to a number of properties, albeit not all. This places the present results on fairly solid ground. Given the general nature of the arguments, the conclusions drawn will be applicable to other systems, with appropriate changes of parameter values. The results provide the basis for assessments of stabilities of particles when a strong radiative cooling is present and may be technological useful for the production of mass-selected nanoparticles.

AUTHOR INFORMATION

Corresponding Author

*E-mail: KlavsHansen@tju.edu.cn.

ORCID

Klavs Hansen: 0000-0001-9746-3711

Notes

The authors declare no competing financial interest.

ACKNOWLEDGMENTS

This work has been supported by the Tianjin International Center of Nanoparticles and Nanosystems, by the Research Foundation-Flanders (FWO), and by the KU Leuven Research Council (GOA/14/007). P.F. acknowledges CONICyT for Becas Chile scholarship.

REFERENCES

(1) Haruta, M. Size-and support-dependency in the catalysis of gold. *Catal. Today* **1997**, *36*, 153−166.

(2) Häkkinen, H.; Abbet, S.; Sanchez, A.; Heiz, U.; Landman, U. Structural, Electronic, and Impurity-Doping Effects in Nanoscale Chemistry: Supported Gold Nanoclusters. *Angew. Chem., Int. Ed.* **2003**, *42*, 1297−1300.

(3) Häkkinen, H. The gold sulfur interface at the nanoscale. *Nat. Chem.* **2012**, *4*, 443−445.

(4) Collings, B. A.; Athanassenas, K.; Lacombe, D.; Rayner, D. M.; Hackett, P. A. Optical absorption spectra of Au_7, Au_9, Au_{11}, and Au_{13}, and their cations: Gold clusters with 6, 7, 8, 9, 10, 11, 12, and 13 s electrons. *J. Chem. Phys.* **1994**, *101*, 3506−3513.

(5) Schweizer, A.; Weber, J. M.; Gilb, S.; Schneider, H.; Schooss, D.; Kappes, M. M. Electronic photodissociation spectroscopy of $Au_4^+Ar_n$, n = 0−4: Experiment and theory. *J. Chem. Phys.* **2003**, *119*, 3699−3710.

(6) Gilb, S.; Jacobsen, K.; Schooss, D.; Furche, F.; Ahlrichs, R.; Kappes, M. M. Electronic photodissociation spectroscopy of Au_n^- Xe (n = 7−11) versus time-dependent density functional theory prediction. *J. Chem. Phys.* **2004**, *121*, 4619−4627.

(7) Lecoultre, S.; Rydlo, A.; Félix, C.; Buttet, J.; Gilb, S.; Harbich, W. UV-visible absorption of small gold clusters in neon: Au_n (n = 1−5 and 7−9). *J. Chem. Phys.* **2011**, *134*, 074302.

(8) Link, S.; El-Sayed, M. Size and Temperature Dependence of the Plasmon Absorption of Colloidal Gold Nanoparticles. *J. Phys. Chem. B* **1999**, *103*, 4212−4217.

(9) Gilb, S.; Weis, P.; Furche, F.; Ahlrichs, R.; Kappes, M. M. Structures of small gold cluster cations (Au_n^+, $n \leq 14$): Ion mobility measurements versus density functional calculations. *J. Chem. Phys.* **2002**, *116*, 4094−4101.

(10) Vogel, M.; Hansen, K.; Herlert, A.; Schweikhard, L. Model Free Determination of Dissociation Energies of Polyatomic Systems. *Phys. Rev. Lett.* **2001**, *87*, 013401.

(11) Hansen, K.; Herlert, A.; Schweikhard, L.; Vogel, M. Dissociation energies of gold clusters Au_N^+, N = 7−27. *Phys. Rev. A: At., Mol., Opt. Phys.* **2006**, *73*, 063202.

(12) Hansen, K.; Ferrari, P.; Janssens, E.; Lievens, P. Extremely High Thermal Radiation of Mass Selected Gold Clusters, to be published.

(13) Ferrari, P.; Janssens, E.; Lievens, P.; Hansen, K. Thermal radiation and fragmentation pathways of photo-excited silicon clusters. *J. Chem. Phys.* **2015**, *143*, 224313.

(14) Hansen, K.; Li, Y.; Kaydashev, V.; Janssens, E. Thermal radiation of laser heated niobium clusters Nb_N^+, $8 \leq N \leq 22$. *J. Chem. Phys.* **2014**, *141*, 024302.

(15) Ito, G.; Furukawa, T.; Tanuma, H.; Matsumoto, J.; Shiromaru, H.; Majima, T.; Goto, M.; Azuma, T.; Hansen, K. Cooling Dynamics of Photoexcited C_6^- and C_6H^-. *Phys. Rev. Lett.* **2014**, *112*, 183001.

(16) Kono, N.; Furukawa, T.; Tanuma, H.; Matsumoto, J.; Shiromaru, H.; Azuma, T.; Najafian, K.; Pettersson, M. S.; Dynefors, B.; Hansen, K. Inverse internal conversion in C_4^- below the electron

DOI: 10.1021/acs.jpcc.6b09998
J. Phys. Chem. C 2017, 121, 10663−10669

detachment threshold. *Phys. Chem. Chem. Phys.* **2015**, *17*, 24732−24737.
(17) Martin, S.; Bernard, J.; Bredy, R.; Concina, B.; Joblin, C.; Ji, M.; Ortega, C.; Chen, L. Fast Radiative Cooling of Anthracene Observed in a Compact Electrostatic Storage Ring. *Phys. Rev. Lett.* **2013**, *110*, 063003.
(18) Rohlfing, E. Optical emission studies of atomic, molecular, and particulate carbon produced from a laser vaporization cluster source. *J. Chem. Phys.* **1988**, *89*, 6103.
(19) Weber, B.; Scholl, R. A new kind of light-generation mechanism: Incandescent radiation from clusters. *J. Appl. Phys.* **1993**, *74*, 607−613.
(20) Nitzan, A.; Jortner, J. Theory of inverse electronic relaxation. *J. Chem. Phys.* **1979**, *71*, 3524−3532.
(21) Messiah, A. *Quantum Mechanics*; North-Holland: Amsterdam, 1961.
(22) Polfer, N.; Oomens, J. Vibrational spectroscopy of bare and solvated ionic complexes of biological relevance. *Mass Spectrom. Rev.* **2009**, *28*, 468−494.
(23) Asmis, K. Structure characterization of metal oxide clusters by vibrational spectroscopy: possibilities and prospects. *Phys. Chem. Chem. Phys.* **2012**, *14*, 9270−9281.
(24) Kaydashev, V.; Ferrari, P.; Heard, C.; Janssens, E.; Johnston, R. L.; Lievens, P. Optical absorption of small palladium-doped gold clusters. *Part. Part. Syst. Char.* **2016**, *33*, 364−372.
(25) Bouwen, W.; Thoen, P.; Vanhoutte, F.; Bouckaert, S.; Despa, F.; Weidele, H.; Silverans, R. E.; Lievens, P. Production of bimetallic clusters by a dual-target dual-laser vaporization source. *Rev. Sci. Instrum.* **2000**, *71*, 54−58.
(26) Vogel, M.; Herlert, A.; Schweikhard, L. Photodissociation of Small Group-11 Metal Cluster Ions: Fragmentation Pathways and Photoabsorption Cross Sections. *J. Am. Soc. Mass Spectrom.* **2003**, *14*, 614−621.
(27) Hansen, K. Statistical Emission Processes of Clusters. *Philos. Mag. B* **1999**, *79*, 1413.
(28) Morse, M. Clusters of transition metal atoms. *Chem. Rev.* **1986**, *86*, 1049−1109.
(29) Abramowitz, M.; Stegun, I. A. *Handbook of Mathematical Functions with Formulas, Graphs, and Mathematical Tables*, 9th ed.; Dover: New York, 1964.
(30) Katakuse, I.; Ichihara, T.; Fujita, Y.; Matsuo, T.; Sakurai, T.; Matsuda, H. Mass distributions of copper, silver and gold clusters and electronic shell structure. *Int. J. Mass Spectrom. Ion Processes* **1985**, *67*, 229−236.
(31) Schweikhard, L.; Hansen, K.; Herlert, A.; Herráiz Lablanca, M.; Marx, G.; Vogel, M. Recent gold cluster studies in a Penning trap. *Int. J. Mass Spectrom.* **2002**, *219*, 363.
(32) Hansen, K. *Statistical Physics of Nanoparticles in the Gas Phase*; Springer: Dordrecht, The Netherlands, 2013.

DOI: 10.1021/acs.jpcc.6b09998
J. Phys. Chem. C 2017, 121, 10663−10669